*Journal of Experimental Botany*, Vol. 70, No. 10 pp. 2665–2681, 2019
doi:10.1093/jxb/erz097 Advance Access Publication 1 March 2019
This paper is available online free of all access charges (see https://academic.oup.com/jxb/pages/openaccess for further details)

RESEARCH PAPER

# The chaperone-like protein CDC48 regulates ascorbate peroxidase in tobacco

**Hervé Bègue[1], Angélique Besson-Bard[1,], Cécile Blanchard[1], Pascale Winckler[2,], Stéphane Bourque[1,], Valérie Nicolas[1], David Wendehenne[1,*,] and Claire Rosnoblet[1,*,]**

[1] Agroécologie, AgroSup Dijon, CNRS, INRA, Université Bourgogne, Université Bourgogne Franche-Comté, F-21000 Dijon, France
[2] Plateforme Dimacell/Imagerie spectroscopique UMR Procédés Alimentaires et Microbiologiques Equipe Procédés Microbiologiques et Biotechnologiques, AgroSup Dijon Nord, 21000 Dijon, France

* Correspondence: david.wendehenne@inra.fr or claire.rosnoblet@inra.fr

Received 15 June 2018; Editorial decision 20 February 2019; Accepted 27 February 2019

Editor: Christine Foyer, Leeds University, UK

## Abstract

**There is increasing evidence that the chaperone-like protein CDC48 (cell division cycle 48) plays a role in plant immunity. Cytosolic ascorbate peroxidase (cAPX), which is a major regulator of the redox status of plant cells, has previously been shown to interact with CDC48. In this study, we examined the regulation of cAPX by the ATPase NtCDC48 during the cryptogein-induced immune response in tobacco cells. Our results not only confirmed the interaction between the proteins but also showed that it occurs in the cytosol. cAPX accumulation was modified in cells overexpressing NtCDC48, a process that was shown to involve post-translational modification of cAPX. In addition, cryptogein-induced increases in cAPX activity were suppressed in cells overexpressing NtCDC48 and the abundance of the cAPX dimer was below the level of detection. Furthermore, the levels of both reduced (GSH) and oxidized glutathione (GSSG) and the GSH/GSSG ratio decreased more rapidly in response to the elicitor in these cells than in controls. A decrease in cAPX activity was also observed in response to heat shock in the cells overexpressing NtCDC48, indicating that the regulation of cAPX by NtCDC48 is not specific to the immune response.**

**Keywords:** Ascorbate peroxidase, CDC48, cryptogein, plant biochemistry, protein–protein interaction, redox regulation, tobacco.

## Introduction

In animals, p97, or valosin-containing protein (VCP, or CDC48 in yeast), is a well described chaperone-like protein involved in numerous cellular activities such as ubiquitin proteasome system (UPS) degradation (Baek *et al.*, 2013). Several studies have reported that VCP/CDC48 recognizes and interacts with poly-ubiquitinated proteins intended for degradation by the proteasome. The energy generated through the ATPase activity of VCP/CDC48 enables the segregation of target proteins from complexes or cellular structures and remodels them. The target proteins are then presented to the proteasome (Wang

Abbreviations: ASA, ascorbate; CDC48, cell division cycle 48; CDNB, 1-chloro-2,4-dinitrobenzene; CFP, cyan fluorescent protein; cAPX, cytosolic ascorbate peroxidase; flg22, flagellin 22; FLIM, fluorescence lifetime imaging; GR, glutathione reductase; GSH, glutathione; GS, glutathione synthase; GSSG, oxidized glutathione; GST, glutathione *S*-transferase; HMW, high molecular weight; HS, heat shock; IB, immunoblot; IP, immunoprecipitation; MAPK, MAP kinase; NEM, N-ethylmaleimide; NO, nitric oxide; PCD, programmed cell death; PIC, protease inhibitor cocktail; PTM, post-translational modification; ROS, reactive oxygen species; TAP, tandem affinity purification; UPS, ubiquitin proteasome system degradation; VCP, valosin-containing protein; YFP, yellow fluorescent protein.

et al., 2004). CDC48 is also conserved in plants, but its functions remain poorly understood compared to yeast and mammals (Bègue et al., 2017). Nevertheless, recent investigations have shown that CDC48A, one of the five isoforms of CDC48 found in *Arabidopsis thaliana*, contributes to lipid-droplet stability through segregation of ubiquitinated oleosins (Deruyffelaere et al., 2018; Kretzschmar et al., 2018). An increasing number of studies have provided evidence that CDC48 contributes to plant immunity. In particular, AtCDC48A has been shown to drive the proteasomal degradation of poly-ubiquitinated SNC1, an intracellular immune receptor involved in resistance against the oomycete *Hyaloperonospora arabidopsidis* Noco2 (Copeland et al., 2016). The corresponding transcripts of AtCDC48B, a second Arabidopsis isoform, were also found to accumulate in the response to the *Oilseed rape mosaic virus* (Niehl et al., 2012). AtCDC48B interacts with the virus-encoded movement protein, promoting its degradation. NtCDC48 is specifically *S*-nitrosylated in tobacco cells undergoing an immune response induced by cryptogein, a protein secreted by the oomycete *Phytophthora cryptogea* that triggers a hypersensitive response in the form of programmed cell death (PCD) to confine the pathogen to restricted necrotic lesions, and that also triggers a systemic acquired resistance that temporarily protects the plant against further infections (Astier et al., 2012; Wendehenne et al., 2014). This nitric oxide (NO)-dependent post-translational modification (PTM) leads to a decrease of the ATPase activity *in vitro* (Astier et al., 2012). Other examples of the involvement of NtCDC48 in plant immunity have been reported. Rosnoblet et al. (2017) demonstrated that NtCDC48 accumulates in cryptogein-treated cells, both at the protein and transcript levels, with the protein being found in an active homohexameric form (the monomer is not able to hydrolysate ATP). We found that cryptogein-induced cell death was accelerated in a cell line overexpressing NtCDC48, supporting a role for it in the hypersensitive response.

Using an immunoprecipitation-based strategy in tobacco, Rosnoblet et al. (2017) identified ~100 putative NtCDC48 protein partners, with functions related to metabolism, intracellular traffic, and (as expected) protein quality control and degradation. Interestingly, this analysis also determined that NtCDC48 interacts with three main proteins involved in redox control, namely catalase, superoxide dismutase, and cytosolic ascorbate peroxidase (cAPX). This is particularly relevant with regard to the crucial functions of reactive oxygen species (ROS) in plant immunity and, more generally, in plant signaling (Mittler et al., 2004; Noctor et al., 2018). Indeed, plants have evolved efficient antioxidant systems to regulate the steady-state level of ROS. Among them, the ascorbate–glutathione cycle is one of the major $H_2O_2$ scavenging systems (Asada, 1999). The first reaction, catalysed by APX, consists of the reduction of $H_2O_2$ to water with ascorbate (ASA) as the specific electron donor. The last enzyme involved in this cycle is glutathione reductase (GR), which catalyses the reduction of oxidized glutathione (GSSG) into reduced glutathione (GSH) and is necessary for the regeneration of ASA.

In plants, several isoforms of APX have been identified, including cytosolic (cAPX), microsomal, and chloroplastic (thylakoid-bound and stromal). In *Nicotiana tabacum*, only one cytosolic, one stromal, and one thylakoid-bound isoform have been identified (Orvar and Ellis, 1995; Mano et al., 1997; Madhusudhan et al., 2003). The isoforms differ not only in their subcellular localization, but also in their molecular weight, three-dimensional structure, and enzymatic features (Anjum et al., 2016). Involvement of APXs in plant immunity is well documented (Mittler et al., 1998; Fujiwara et al., 2016; Chen et al., 2018),and it has been shown that modulation of the transcription, translation, and/or activity of APX is strongly correlated with the responses to microbial pathogens. Moreover, APX is subject to several forms of PTM. For instance, in *Antiaris toxicaria*, an excess of $H_2O_2$ during seed desiccation leads to the carbonylation of APX residues and to an irreversible inhibition of its activity (Bai et al., 2011). APX is also prone to phosphorylation. For example, in wheat the protein encoded by the resistance gene *WHEAT KINASE START1* has been shown to phosphorylate thylakoid-bound APX, leading to an inhibition of its enzymatic activity (Gou et al., 2015). It was proposed that this process negatively impacts on the ability of cells to detoxify ROS and that it might contribute to cell death. In addition, NO-mediated PTMs have been reported to influence APX activity. In tobacco, addition of NO donors is followed by an inhibition of APX activity through the reversible binding of NO to the heme prosthetic group (Clark et al., 2000). The incidence of *S*-nitrosylation is more controversial. In *A. toxicaria*, *S*-nitrosylation of cAPX has been shown to prevent its carbonylation and it has been speculated that this mechanism could enhance its activity (Bai et al., 2011). Similarly, in salt-stressed pea plants cAPX activity has been found to be enhanced through *S*-nitrosylation (Begara-Morales et al., 2014). In tobacco cells, a decrease in both the amount and activity of cAPX is observed during the PCD triggered by heat stress. This process is partly linked to reduced expression of the corresponding gene during the late phase of PCD (Vacca et al., 2004). Furthermore, cAPX has been found to undergo *S*-nitrosylation during heat stress. In contrast to the studies detailed above, de Pinto et al. (2013) used *in vitro* and *in vivo* assays to demonstrate that this modification triggers a rapid decrease in cAPX activity and facilitates its degradation through UPS.

In the present study, we investigated the influence of NtCDC48 on cAPX regulation during the immune response triggered by cryptogein in tobacco. We confirmed the interaction between NtCDC48 and cAPX, and found that it occurs in the cytoplasm and independently of the immune response. We provide evidence that cAPX accumulation and activity, and more generally the glutathione status, are strongly affected in cells overexpressing NtCDC48. Collectively, our data demonstrate that CDC48 in an important regulator of cAPX.

## Materials and methods

### Cell treatments

*Nicotiana tabacum* cv. Xanthi wild-type (WT) and NtCDC48-TAP cell suspensions (Rosnoblet et al., 2017) were maintained in the exponential phase growth and sub-cultured 1 d prior to use (Besson-Bard et al., 2008). Cryptogein was purified according to Bonnet et al. (1996). Flagellin 22

(fgl22) from *Xanthomonas campestris* pv campestris was provided by Dr Benoit Poinssot (Agroécologie, Dijon). Cells were treated with 100 nM cryptogein, 1 μM of flg22, or an equal volume of water as a control. Heat shock was applied at 55 °C for 10 min.

### *Immunoblotting*

Proteins from tobacco cells were quantified using the Bradford method (Bradford, 1976) after disruption in lysis buffer, which consisted of 50 mM HEPES, pH 7.5, 50 mM EDTA, 2 mM dithiothreitol (DTT), 100 mM NaCl, and protease inhibitor cocktail (PIC) without EDTA (Roche), either supplemented or not with 10 mM N-Ethylmaleimide (NEM). Protein samples (20 μg) were resolved by 10–15% SDS-PAGE or 6% native-PAGE and visualized by immunoblotting with antibodies against CDC48 (Abcam), cAPX (Agrisera), or His-tag (Cell Signaling Technology). The immunoblots were examined using LumiGLO® (Cell Signaling Technology). After transfer, membranes were stained with Ponceau Red in order to check the loading of total proteins. For gel retardation assays, 12% gels were supplemented with 50 μM Phos-tag™ AAL-107 (Wako Pure Chemical Co.) and 100 μM $MnCl_2$ and then rinsed in 1 mM EDTA for $Mn^{2+}$ chelation.

### *Molecular biology*

Total RNAs were extracted using TRIzol Reagent (Life Technologies) and then 500 ng samples were reverse-transcribed using oligo-dT primer and a DyNamo™ kit (Thermo Fisher Scientific). The reverse-transcriptase quantitative PCR (RT-qPCR) was performed using a SYBR Green PCR Master Mix kit, ViiA™7 apparatus, and v1.2 software (Life Technologies). Samples were log-transformed and normalized to the L25 control (Schmidt and Delaney, 2010). Primers used for PCR and RT-qPCR are listed in Supplementary Table S1 at *JXB* online. The cytosolic cAPX coding sequence was cloned in order to obtain His-tagged or fluorescent proteins. After amplification of inserts from reverse-transcribed mRNA, cAPX constructions were obtained using Gateway BP and LR Clonase kits (Invitrogen) with the plasmids pDONR221 and pHGWA or pH7YWG2 (Nter His or Cter Yellow Fluorescent Protein-tag fusion, Plant System Biology, Ghent, Belgium; Karimi *et al.*, 2005). For cyan fluorescent protein (CFP)-NtCDC48, the LR reaction was performed with the pH7WGC2 plasmid (Nter Cyan Fluorescent Protein-tag fusion; Karimi *et al.*, 2005) from previously cloned NtCDC48 in pENTR (Rosnoblet *et al.*, 2017).

### *Pull-down assays*

Beads linked to recombinant His-NtCDC48 proteins were obtained as previously described (Rosnoblet *et al.*, 2017). Samples of 500 μg of proteins from tobacco cells extracted with immunoprecipitation (IP) buffer (50 mM HEPES pH 7.4, 100 mM NaCl, 1 mM DTT, 4 mM EDTA, 10% sucrose, 0.3% IGEPAL CA-630, 100 μM $Na_3VO_4$, 10 mM beta-glycerophosphate, and PIC) were cleared with 40 μl of free Ni-NTA beads (GE Healthcare) for 3 h. The sample extract was then recovered by centrifugation at 800 *g* at 4 °C, and incubated overnight at 4 °C with 20 μl of 5% His-NtCDC48-beads or free beads as a negative control. After incubation, total lysates were kept as 'posts' in order to check for the absence of protein degradation during incubation. After extensive washing, linked proteins were resolved by 12% SDS-PAGE and then His-NtCDC48 and cAPX were immunoblotted.

### *Co-immunoprecipitation*

Samples of 1 mg of proteins extracted in the IP buffer were incubated with 25 μl of Protein A Mag Sepharose (GE Healthcare) and 1.5 μg of an antibody against CDC48 or against phosphorylated MAP kinases (MAPK) as a negative control (Cell Signaling Technology). After the washing phase, co-immunoprecipitated proteins were resolved by SDS-PAGE and immunoblotted. Protein A coupled with horseradish peroxidase (Abcam) was used instead of a secondary antibody.

### *Fluorescence resonance energy transfer by fluorescence lifetime imaging*

*Agrobacterium tumefaciens* strain (GV3101) was transformed with CFP-NtCDC48 (donor) or cAPX-YFP (acceptor) or both constructions together and then grown at 28 °C with gentamycin (50 μg $ml^{-1}$) and rifampicin (50 μg $ml^{-1}$) for the strain plus spectinomycin (100 μg $ml^{-1}$) for the plasmids. Newly transformed bacteria were then infiltrated into *Nicotiana tabacum* leaves in 10 mM MES, 10 mM $MgCl_2$, and 100 μM acetosyringone using a syringe. Four plants were infiltrated and 15 leaf disks per plant were analysed. Expression of the fluorescent-coupled proteins was checked using an epifluorescence microscope (Leica) 4 d after infiltration.

Fluorescence lifetime imaging (FLIM) images were collected using a time-correlated single-photon counting (TCSPC) module (PicoQuant) on a Nikon A1-MP scanning microscope. Imaging was carried out with a ×60 Apo IR objective (NA: 1.27, Water Immersion, Nikon). Excitation at 820 nm was provided by an IR laser (Chameleon, Coherent) that delivered femtosecond pulses at a repetition rate of 80 MHz. Fluorescence emission of CFP was collected using a Single-Photon Avalanche Diode detector, using a FF01-494/20 band-pass emission filter (Semrock). TCSPC lifetime recording was performed over 200 temporal channels (final resolution 0.64 ps). We performed a global lifetime analysis on regions of interest of the FLIM images using the SymPhoTime software (PicoQuant). The fluorescence lifetimes were calculated by fitting the tail of the CFP fluorescence decay to a biexponential model, with two lifetime constants. For this analysis, we report only the longer lifetime as it was the most sensitive to fluorescence resonance energy transfer (FRET). The efficiency of energy transfer (FRET %) was given by the following equation: $E=[1-(FDA/FD)]\times100$, with relative fluorescence intensities of the donor in the absence (FD) or presence (FDA) of the acceptor.

### *Recombinant cAPX production, purification, and biotin switch*

His-tagged cAPX protein was produced in *E. coli* (Rosetta II) cells grown at 37 °C in Luria-Bertani medium. When the culture reached an optical density (600 nm) of ~0.45, protein production was induced with 1 mM isopropyl 1-thio-β-D-galactopyranoside for 3 h before purification using a His-trap HP column by chromatography on ÄKTApurifier (GE Healthcare). His-cAPX-containing fractions were dialysed against 20 mM $NaH_2PO_4/Na_2HPO_4$, pH 7.0, 200 mM KCl, and 1 mM EDTA. Protein was then concentrated up to 4 μg $\mu l^{-1}$ with an Amicon Ultra centrifugal filter (cut-off 10 kDa; Merck Millipore). Samples of 10 μg of recombinant cAPX were treated overnight with GSSG (500 μM) or GSNO (500 μM) and were then subjected to the biotin switch method for the detection of *S*-nitrosylated proteins according to Astier *et al.* (2012). Biotinylation of cAPX was analysed by immunoblotting with peroxidase-coupled anti-biotin antibodies (Sigma Aldrich) or with an antibody against cAPX.

### *Gel filtration*

Cells lysis was performed in gel filtration buffer (20 mM HEPES-KOH pH 7.6, 5% glycerol, 100 mM KCl, 1 mM DDT, 1 mM $Na_3VO_4$, 1 mM EDTA, and PIC) supplemented with 10 mM NEM. After centrifugation for 10 min at 20 800 *g* at 4 °C, 500 μg of extracts were fractionated on a Superdex 200HR column and chromatography was carried out on HPLC ÄKTApurifier (GE Healthcare). Blue dextran (V0), ferritin (440 kDa), aldolase (158 kDa), conalbumine (75 kDa), ovalbumine (43 kDa), and cytochrome c (14 kDa) were used for calibration. Collected fractions were precipitated in trichloroacetic acid and then examined by immunoblotting.

### *cAPX activity*

Cells were homogenized in extraction buffer (100 mM potassium phosphate pH 7, 0.1 mM EDTA, 0.1 mM ascorbate, and 1%

polyvinylpyrrolidone) then centrifuged at 16 000 *g* for 15 min at 4 °C. APX activity (EC 1.11.1.11) was analysed as described by Vacca *et al.* (2004). Decrease of absorbance at 290 nm was measured in an activity mix (20 µl of supernatant, 50 mM potassium phosphate, pH 7.0, 0.01 mg BSA, 0.5 mM ascorbate) after addition of 0.25 mM $H_2O_2$.

### *Ascorbate and glutathione assays*

Cells were homogenized in 0.2 M HCl. After centrifugation for 10 min at 16 000 *g* at 4 °C, neutralized supernatants were used for assays for both ascorbate and glutathione. Contents of ascorbate (ASA), total ascorbate (dehydroascorbate+ASA), glutathione (GSSG), and total glutathione (GSH+GSSG) were determined according to Noctor *et al.* (2016). The method allows the GSH content to be deduced [=total glutathione–(2×GSSG)]. The amounts of ascorbate and glutathione were expressed in micromoles or nanomoles of ascorbate or glutathione per gram fresh weight (FW). Percentage GSH was calculated as (GSH/total glutathione)×100 and the GSH/GSSG ratio was also determined (Queval and Noctor, 2007).

### *GR activity*

The activity of glutathione reductase (GR) was quantified according to Murshed *et al.* (2008). Briefly, cells were lysed in 50 mM MES-KOH pH 6, 40 mM KCl, 2 mM $CaCl_2$, and 1 mM L-ascorbic acid. After centrifugation for 10 min at 16 000 *g* and 4 °C, the GR activity was measured through NADPH oxidation using absorbance at 340 nm in 50 mM HEPES pH 8, 0.5 mM EDTA, 0.25 mM NADPH, and 0.5 mM GSSG.

### *GST activity*

The activity of glutathione *S*-transferase (GST) was quantified through the ability of glutathione to conjugate 1-chloro-2,4-dinitrobenzene (CDNB; Sigma Aldrich). Cells were lysed in extraction buffer (50 mM potassium-phosphate, pH 7.2, 2 mM DTT, 0.01% triton X-100, and 1 mM EDTA) and the supernatant was used after centrifugation for 30 min at 25 000 *g* at 4 °C. GST activity was measured in 200 µl of extraction buffer, 2 mM GSH, and 10 µl of cell lysate. The reaction was started with 1 mM CDNB then allowed to progress for 30 min at 30 °C. Activity was determined by following the increase in absorbance at 340 nm.

## Results

### *cAPX interacts with NtCDC48*

In a previous study, we identified cAPX as a putative partner of NtCDC48 under basal conditions and during the immune response triggered by cryptogein (Supplementary Fig. S1; Rosnoblet *et al.*, 2017). In order to confirm the interaction between the proteins, several complementary approaches were performed. First, a pull-down strategy was carried out, in which a His-tagged NtCDC48 recombinant protein was produced in *E. coli*, purified, and fixed by affinity on Ni-NTA beads. These were then incubated with proteins extracted from wild-type (WT) cells elicited by cryptogein.

We checked that His-NtCDC48 was only detected in NtCDC48-linked beads by immunoblotting (Fig. 1A). Using an antibody against His-tag, the recombinant His-NtCDC48 was detected in its monomeric (90 kDa) and tightly bound hexameric forms (>250 kDa) as previously reported (Rosnoblet *et al.*, 2017). Immunoblots raised against cAPX then showed that the endogenous cAPX was detected exclusively in the total lysates, in pull-downs with His-NtCDC48 beads, and in the 'posts', whatever the cryptogein elicitation time. Thus, cAPX interacted *in vitro* with the recombinant protein His-NtCDC48, and this interaction was not affected by the cryptogein treatment.

To determine whether the endogenous NtCDC48 protein also interacted with cAPX, we performed a co-IP experiment in WT cells elicited by cryptogein (Fig. 1B). In the total lysates, an increased accumulation of NtCDC48 in its hexameric form was observed during elicitation, confirming our previous study that showed that cryptogein triggers an accumulation of NtCDC48 (Rosnoblet *et al.*, 2017). Moreover, following immunoblotting against endogenous cAPX in the total lysates, we observed two immunoreactive bands with molecular masses estimated at ~31 kDa and ~33 kDa; a 28 kDa size would be expected in theory for cAPX (Orvar and Ellis, 1995). These two immune-reactive signals were detected at all time points after IP of NtCDC48 followed by immunoblotting against cAPX (Fig. 1B). This confirmed the *in vivo* interaction between the proteins and also indicated that it occurred independently of the cryptogein treatment.

As controls, we verified that cAPX was co-immunoprecipitated through CDC48 antibodies but not after incubation with free beads or using neutral antibodies, for example those raised against phosphorylated MAPK. The latter were not shown to interact with cAPX or CDC48. As expected, cAPX did not stick to free beads and was not co-immunoprecipitated through phospho-MAPK antibodies (Fig. 1D).

To examine whether the overexpression of NtCDC48 could affect its interaction with cAPX, we performed a similar experiment in the NtCDC48-TAP line overexpressing NtCDC48, which we had previously characterized (Rosnoblet *et al.*, 2017). In these cells, cAPX was also found among the proteins co-immunoprecipitated through NtCDC48 (Fig. 1C). However, compared to WT cells, the 33 kDa signal was more predominant both in the total lysate and following co-IP. Moreover, a decreased amount of cAPX was observed between 2 h and 12 h of cryptogein incubation. It should be noted that with the extracts from NtCDC48-TAP cells we were not able to perform a negative control using phospho-MAPK antibodies because of the Igg-binding domain in the tag. However, we determined that cAPX extracted from overexpressing cells did not stick to free beads (Fig. 1C).

The interaction between cAPX and NtCDC48 was then studied *in planta* using FRET with FLIM. Using agro-infiltration, we transiently expressed the CFP-NtCDC48 and cAPX-YFP proteins in *N. tabacum* cv. Xanthi leaves. As expected from their subcellular localization, cAPX-YFP was only detectable in the cytoplasm while CFP-NtCDC48 was observed in the cytoplasm and in the nucleus (Supplementary Fig. S2). Thus, both proteins co-localized in the cytoplasm, and we then looked for their molecular interaction using FLIM. In the leaf epidermal cells expressing only the CFP-NtCDC48 protein, the fluorescence was detected in the cytoplasm and the nucleus with a mean lifetime of 2.97 ns for CFP without a partner (Fig. 2A, B). In these cells, the fluorescence lifetimes measured in the nucleus and cytoplasm were similar to the global measurement. In leaves co-expressing CFP-NtCDC48 and cAPX-YFP, the CFP lifetime was significantly reduced to 2.41 ns (Fig. 2B). This reduction was due to the transfer

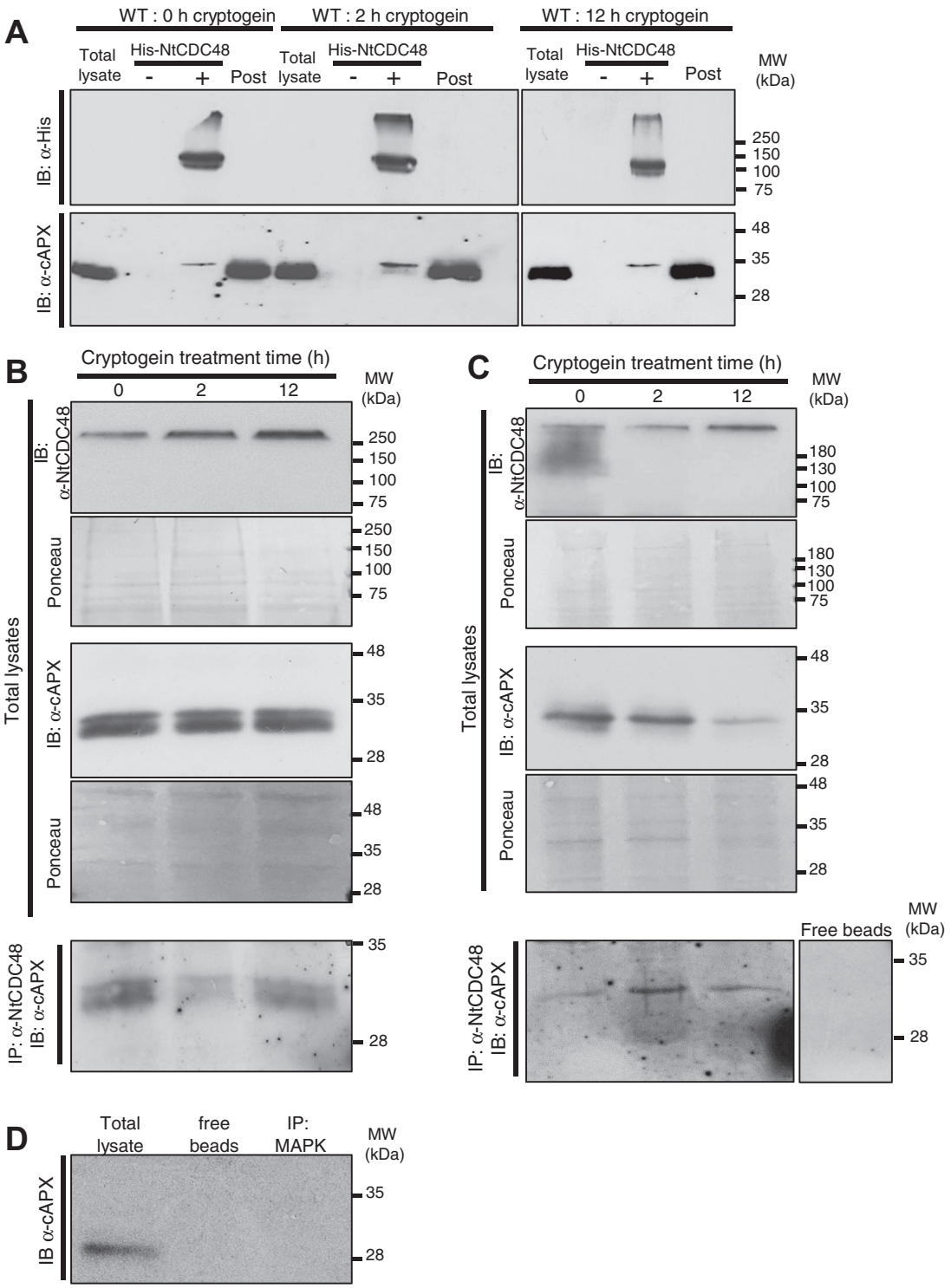


**Fig. 1.** Interactions between cAPX and NtCDC48. (A) Pull-down assays of cAPX with His-NtCDC48 beads. His-NtCDC48 recombinant proteins were fixed on Ni-NTA affinity beads and incubated with proteins extracted from wild-type (WT) tobacco cells treated with 100 nM cryptogein. The negative control was performed with Ni-NTA beads without His-NtCDC48. The immunoblots detected His-Tag and cAPX. After incubation of protein extracts with the beads, the total lysates were loaded in gels as 'posts' in order to check for the absence of protein degradation. (B, C) Immunoprecipitation (IP) of NtCDC48 proteins followed by immunoblotting raised against cAPX. Proteins were extracted from WT (B) and NtCDC48-TAP (C) cells treated with 100 nM cryptogein for the indicated times. The presence of NtCDC48 and cAPX in the total lysates and in IP were detected by immunoblotting against endogenous proteins. The Ponceau staining shows equal protein loading of the total lysates. As negative controls for NtCDC48-TAP cells, proteins were incubated with magnetic beads without the antibody. (D) Negative controls for WT cells. Protein extracts were incubated with free beads or subjected to IP through an antibody raised against phosphorylated MAPK followed by immunoblotting targeting cAPX. The results shown are representative of three replicates. MW, molecular weight.

A

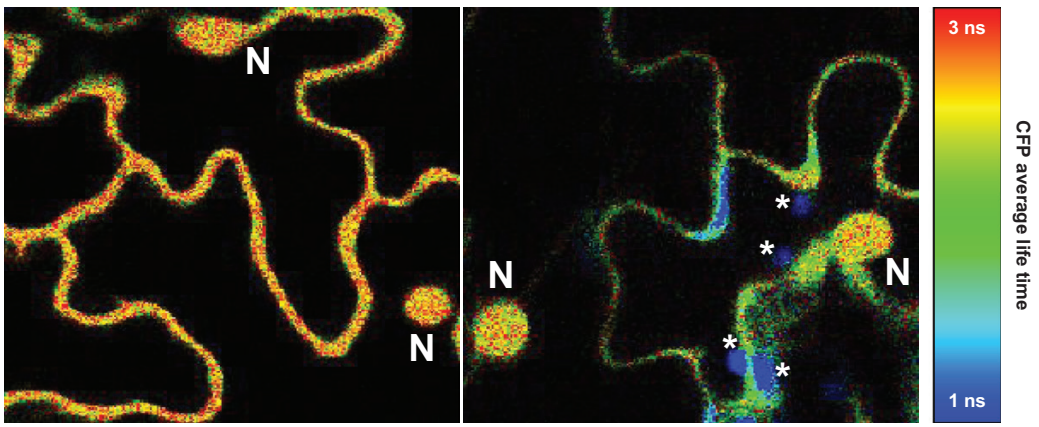


B

| Donor | Acceptor | N | Average τ (ns) | SEM | FRET (%) | p-value |
|---|---|---|---|---|---|---|
| CFP-NtCDC48 | - | 23 | 2.97 | 0.04 | - | - |
| CFP-NtCDC48 | cAPX-YFP | 25 | 2.41 | 0.04 | 19.0 | $1.21e^{-13}$ |

**Fig. 2.** Interaction between cAPX and NtCDC48 in tobacco leaves detected by fluorescence resonance energy transfer–fluorescence lifetime imaging (FRET–FLIM). (A) Representative FLIM images of cells expressing CFP-NtCDC48 alone (donor, left) or CFP-NtCDC48 and the acceptor cAPX-YFP (right). The scale on the left indicates the cyan fluorescent protein (CFP) lifetime, ranging from 1–3 ns. N, nucleus. Asterisks indicate the fluorescence lifetime signal of the chloroplast autofluorescence. (B) FLIM analysis of CFP-NtCDC48 alone and together with cAPX-YFP. N, number of measurements; Average τ, CFP mean lifetime; SEM, standard error of the mean; FRET (%), percentage of FRET efficacity. Statistical analysis was carried out using a *t*-test. (This figure is available in colour at *JXB* online.)

of fluorescence resonance energy to cAPX-YFP and was observed in the cytoplasm but not in the nucleus (Fig. 2A). These results strongly suggested that NtCDC48 and cAPX interact exclusively in the cytoplasm. We had also planned to perform a FLIM experiment in tissues pre-infiltrated with cryptogein; however, these assays were not successful because of the disruption of the tissues associated with cryptogein injection (Xing *et al.*, 2016).

### *Analysis of cAPX dynamics*

In order to understand the functional relationship between CDC48 and cAPX, we analysed the accumulation of cAPX transcripts and proteins during the immune response triggered by cryptogein in WT and in NtCDC48-TAP tobacco cell lines. In both cases, cryptogein induced a significant increase in *cAPX* transcript levels after 4 h of treatment, and the levels further increased with time (Fig. 3A, B). At the protein level, as already shown in Fig. 1B, two immunoreactive bands of ~31 kDa and ~33 kDa were detected with the antibody raised against cAPX (Fig. 3C). In WT cells without cryptogein treatment, the 31 kDa signal was predominant and showed a slight accumulation at 12 h. In cryptogein-treated WT cells, increasing amounts of the two bands were observed during the time course of elicitation. Interestingly, a distinct profile of cAPX accumulation occurred in the NtCDC48 overexpressing line. Without cryptogein treatment, the 33-kDa band was predominant while the 31 kDa signal was hardly detected. Furthermore, and in contrast to WT cells, cryptogein treatment did not induce increased accumulation of cAPX, and the 33-kDa signal slightly decreased after 6 h of elicitation (Fig. 3C). Over a longer time period, a decrease in the accumulation of the cAPX signal was observed in both the WT and the overexpressing lines. Overall, these results indicated that the overexpression of NtCDC48 affects cAPX accumulation, both qualitatively and quantitatively.

Since cAPX has been shown to be phosphorylated (Gou *et al.*, 2015), the mass increment of the 33 kDa signal could be linked to this form of post-translational modification (PTM) To check this hypothesis, we performed Phos-tag SDS-PAGE retardation assays (Fig. 4), which considerably slows down the electrophoretic migration of phosphorylated polypeptides. The migration of the cAPX signals in the Phos-tag gels, did not change in comparison to SDS-PAGE (Fig. 4A). We carried out immunoblotting against phosphorylated MAPK as a positive control. As expected, phosphorylation of MAPK occurred after 2 h of cryptogein treatment and the Phos-tag gels revealed a clear electrophoretic retention (Fig. 4B). Taken together, these results indicated that the differences in electrophoretic mobility observed between the two cAPX signals were not due to phosphorylation.

In addition to phosphorylation, APX can be subject to PTM induced by reactive oxygen or nitrogen species (Clark *et al.*, 2000; Lozano-Juste *et al.*, 2011; Gou *et al.*, 2015), with these modifications mainly affecting Met or Cys residues. To determine whether the 33-kDa band could correspond to such a modification,

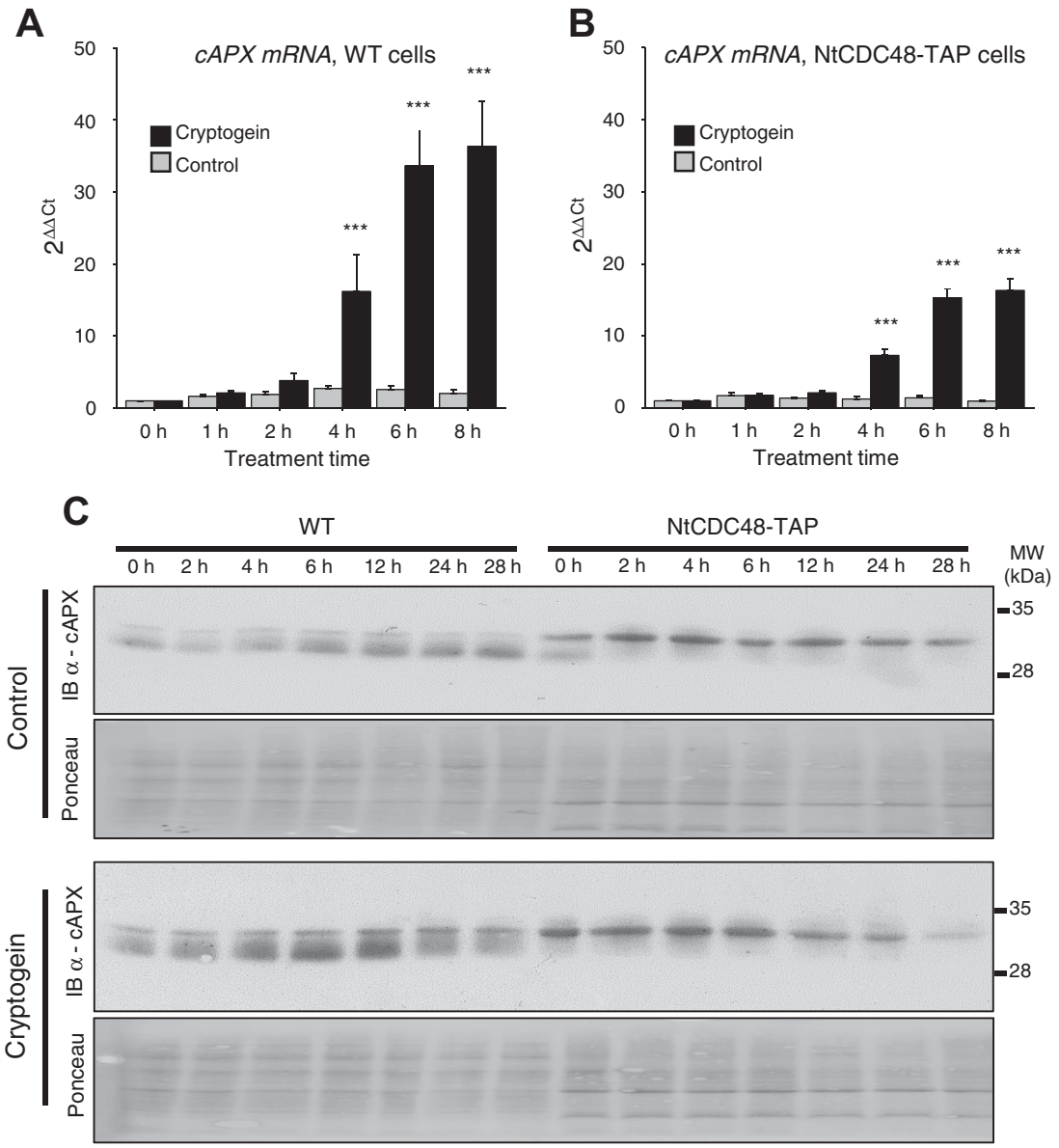


**Fig. 3.** cAPX transcripts and protein accumulation in wild-type (WT) and NtCDC48-TAP tobacco cells. The amount of *cAPX* mRNA was measured in WT (A) and NtCDC48-TAP (B) cells elicited with 100 nM cryptogein. Accumulation of *cAPX* mRNA was analysed by reverse-transcriptase quantification PCR (RT-qPCR) using *L25* mRNA as the calibrator gene. Five independent experiments were performed. Data are means (±SE) and significant differences between treatment and control were determined using ANOVA followed by Fisher's range test (***$P$<0.001). (C) Time course of cAPX protein accumulation. WT and NtCDC48-TAP cells were treated with 100 nM cryptogein or an equivalent volume of water as a control, 20 µg of extracted proteins were separated by SDS-PAGE, and endogenous cAPX was analysed by immunoblotting (IB, upper panels). Protein loading was checked using Ponceau staining (bottom panels). The results are representative of five independent experiments.

protein extracts from control and cryptogein-treated WT and transgenic cells were incubated with N-ethylmaleimide (NEM), an alkylating reagent that reacts with Cys residues (Paulech *et al.*, 2013). Immunoblotting against cAPX showed that the NEM treatment strongly affected the presence of the 33-kDa immunoreactive polypeptide (Fig. 5). In WT cells, compared to samples not treated with NEM (Fig. 3C), this band was hardly observed, even in the cryptogein-treated samples. In the transgenic line, the 31-kDa signal, which was rarely observed in proteins not treated with NEM (Fig. 3C), was clearly detected in both the cryptogein-treated samples and in control samples treated by NEM (Fig. 5). These results strengthened the hypothesis that the 33-kDa and 31-kDa bands correspond to the same polypeptide undergoing a Cys-dependent PTM. Importantly, gel filtration analysis of NEM-treated WT and NtCDC48-TAP samples clearly demonstrated that the distinct electrophoretic mobility of both signals was not due to a mass increment (Fig. 6). The 31-kDa signal was detected in fractions corresponding to higher molecular mass (fractions 7–9) compared to the fractions enriched in the 33-kDa polypeptide (fractions 9–12). Such a phenomenon could be due to steric hindrance linked to oxidative modification.

NEM is a thiol-reacting agent. Since APX has been shown to be modified by *S*-nitrosylation (de Pinto *et al.*, 2013), we examined the influence of cysteine *S*-nitrosylation on cAPX electrophoretic migration using a recombinant

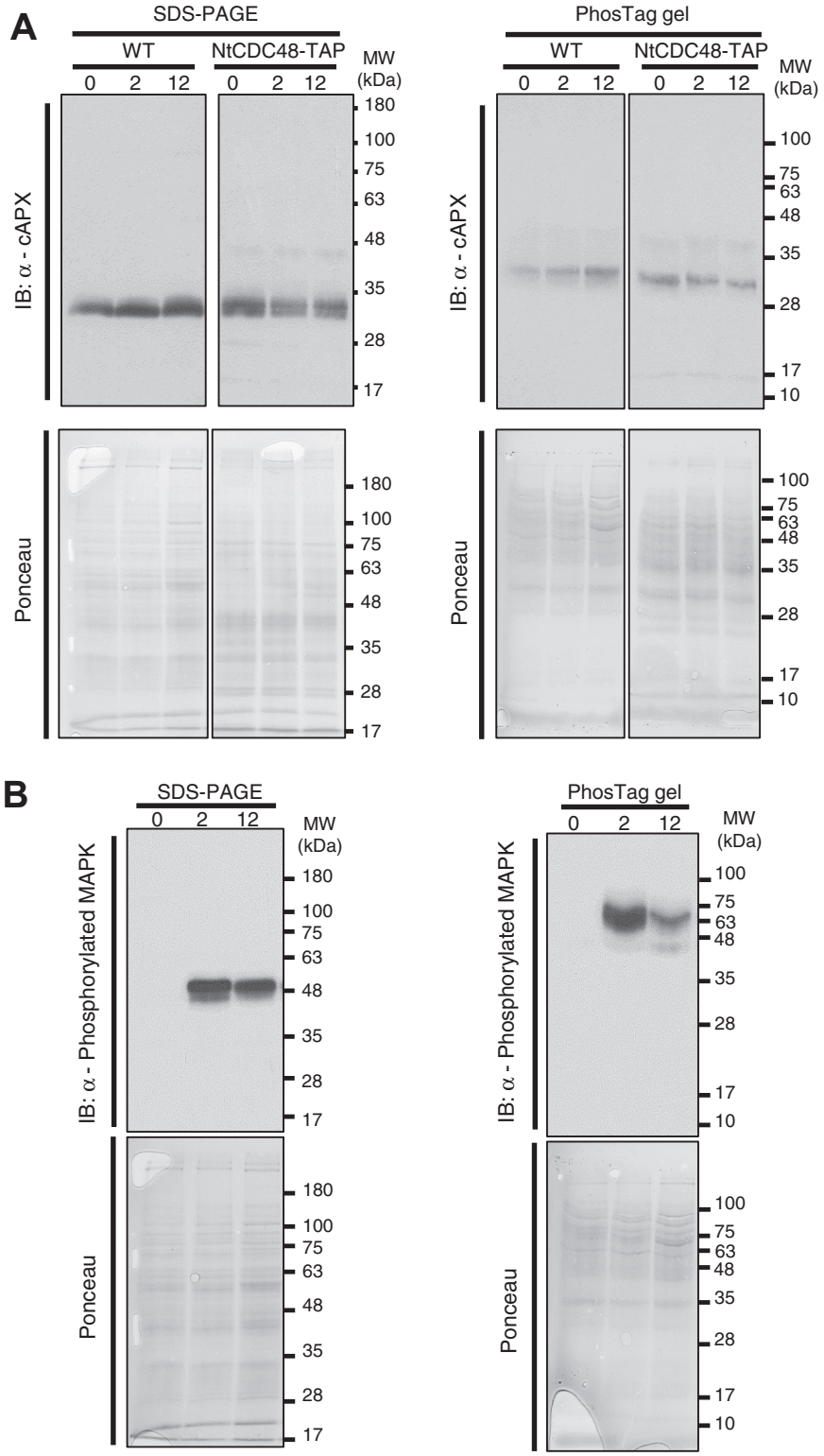


**Fig. 4.** Analysis of cAPX phosphorylation in tobacco cells by gel retardation. (A) Immunoblot against cAPX protein in SDS-PAGE and in gel supplemented with Phos-tag™ AAL-107 in wild-type (WT) and NtCDC48-TAP cells during cryptogein elicitation. The presence of cAPX was detected using an anti-APX antibody. (B) Positive controls were performed with immunoblots raised against phosphorylated MAPK in WT cells. Ponceau staining (lower panels, total lysate) allowed the progress of the whole protein migration to be followed and permitted the equal loading of proteins in the gels to be checked.

protein (Supplementary Fig. S3). First, we confirmed the *in vitro S*-nitrosylation of cAPX and the resulting inhibition of its enzymatic activity (Supplementary Fig. S3A, B) as previously reported (de Pinto *et al.*, 2013). Second, both the non-nitrosylated and the *S*-nitrosylated proteins showed the same electrophoretic migration with an apparent molecular mass of 31 kDa, minimizing the possibility that the 33-kDa signal could correspond to an *S*-nitrosylated cAPX (Supplementary Fig. S3C). We also found that NEM induced a decrease of cAPX activity *in vitro* (Supplementary Fig. S3B), suggesting

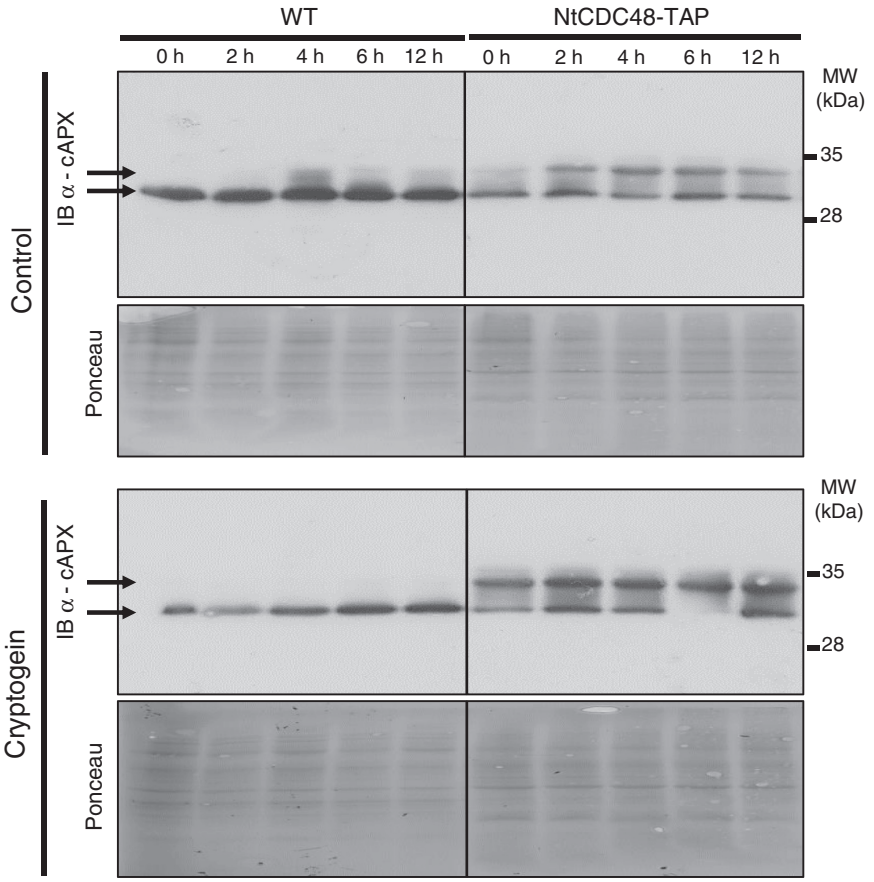


**Fig. 5.** Effect of N-ethylmaleimide (NEM) on cAPX protein electrophoretic migration. Time-course of cAPX protein accumulation. Wild-type (WT) and NtCDC48-TAP tobacco cells were treated with 100 nM cryptogein or an equivalent volume of water as a control. Samples of 20 μg of proteins extracted with buffer supplemented by 10 mM (NEM) were separated by SDS-PAGE, and endogenous cAPX was analysed by immunoblotting (IB, top panels). Protein loading was checked using Ponceau staining (bottom panels). The results are representative of five independent experiments.

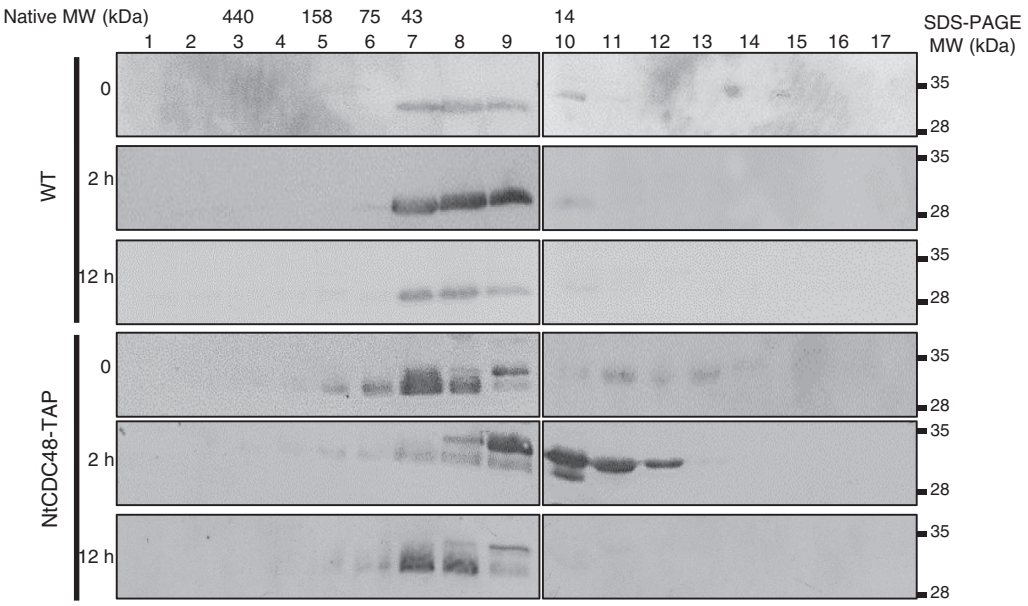


**Fig. 6.** Gel filtration analysis of the two immunoreactive cAPX signals in wild-type (WT) and NtCDC48-TAP tobacco cells. Cells were treated with 10 mM cryptogein and proteins (500 μg) were extracted with buffer supplemented with N-ethylmaleimide (NEM). The proteins were separated according to their molecular weight using gel filtration chromatography. After TCA precipitation of each fraction, cAPX was detected by immunoblot analysis.

that the alkylation induced by NEM affected the Cys residues involved in cAPX activity and/or in the folding of the protein.

To complete the expression analysis, the enzymatic activity of cAPX was measured in the two cell lines with and without cryptogein treatment by following the oxidation of ASA in the

presence of $H_2O_2$. We first checked that the experimental procedure only measured the cytosolic APX activity without any interference from chloroplastic activity (Supplementary Fig. S4). We found that there was no difference between total and cytosolic ascorbate peroxidase activity, with other APXs being inactivated because of the absence of ASA in the extraction buffer and the pre-incubation with $H_2O_2$ (Amako *et al.*, 1994). In WT cells, a significant increase in the activity of cAPX was measured after 2 h of cryptogein treatment (Fig. 7A); however, this increase was only transient and by 4 h the activity had returned to background level. In cells overexpressing NtCDC48 without cryptogein treatment, the rate of cAPX activity was half

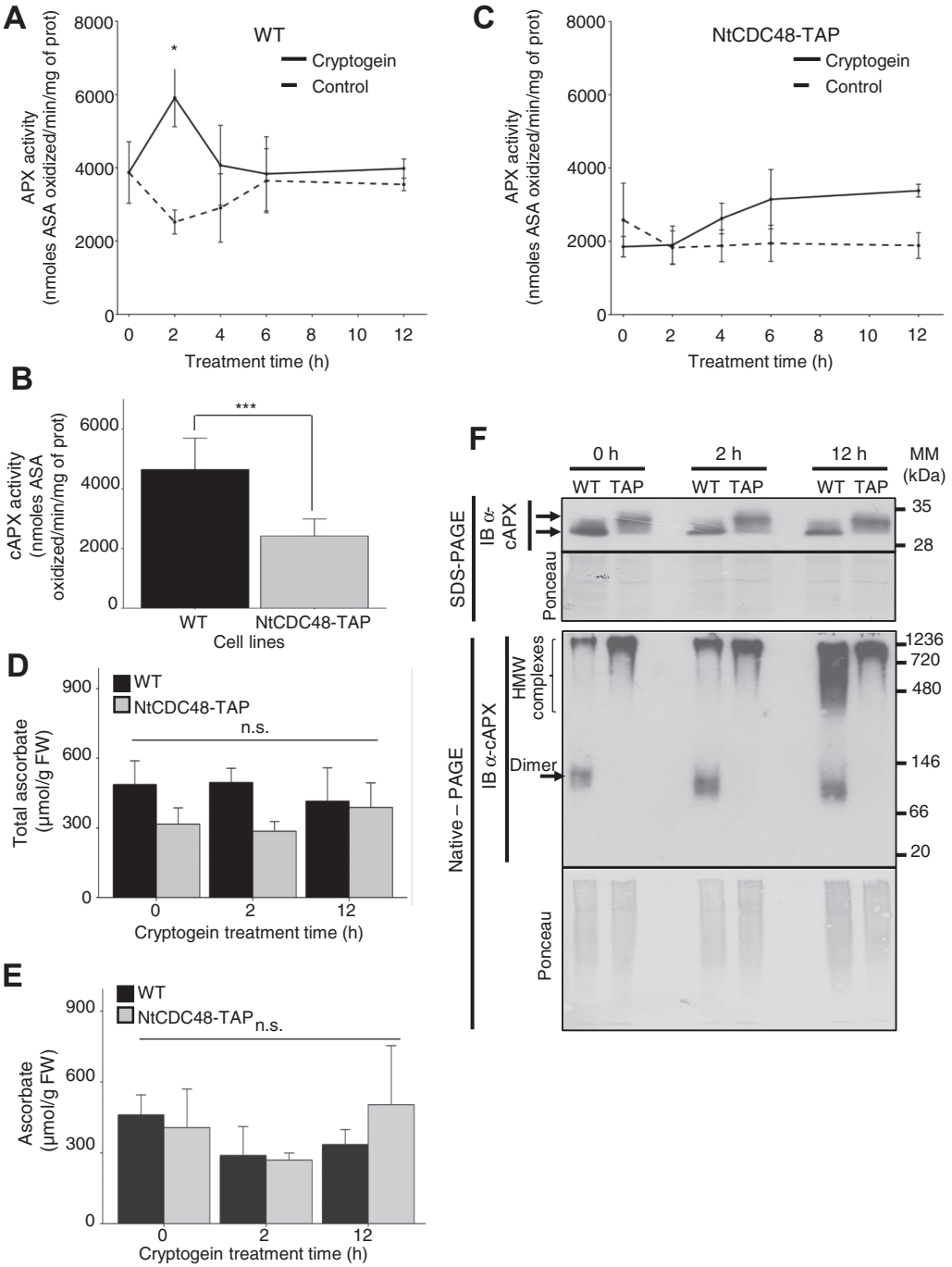


**Fig. 7.** Ascorbate peroxidase activity, quantification of ASA, and native conformation of cAPX in wild-type (WT) and NtCDC48-TAP tobacco cells. APX activity in WT (A) and NtCDC48-TAP cells (C) treated with 100 nM cryptogein or an equivalent volume of water (control). Data are means (±SE) of four biological replicates. Significant differences were determined using Kruskal–Wallis test (*$P$<0.05). (B) Basal activity APX of in WT and NtCDC48-TAP cells. Data are means (±SE) of four biological replicates. The significant difference was determined using a $t$-test ($P$<0.001). (D) Reduced ascorbate and its oxidized form dehydroascorbate, and (E) reduced ascorbate in WT and NtCDC48-TAP cells treated with 100 nM cryptogein. Data are means (±SE) of four biological replicates. n.s., no significant differences between control and treated cells (Wilcoxon test). (F) Native structural conformation of endogenous cAPX. WT and NtCDC48-TAP (TAP) cells were treated with 100 nM cryptogein for the period indicated. Each sample (20 µg) was analysed by immunoblotting with an anti-cAPX antibody after separation using 15% SDS-PAGE under reducing conditions (upper panels) or 6% native-PAGE (lower panels). HMW, high molecular weight. Protein loading was checked using Ponceau staining, shown below each immunoblot.

that of WT cells (Fig. 7B). Interestingly, in contrast to the WT, cryptogein did not induce any significant increase in cAPX activity in the overexpressing line (Fig. 7C). In order to determine whether the differences in cAPX activities observed in the WT and NtCDC48-TAP lines were linked to substrate availability, we determined the level of ascorbate in cells exposed to cryptogein. Similar levels of total and reduced ascorbate were observed irrespective of the cell line and cryptogein elicitation treatment (Fig. 7D, E). Therefore, the absence of induction of cAPX activity observed in NtCDC48-TAP cells exposed to cryptogein was not linked to reduced concentration of ascorbate.

A recent study has shown that rice cAPX is present as a dimer and in high-molecular-weight (HMW) complexes (Hong *et al.*, 2018). The dimer displays high peroxidase activity while the HMW complexes function predominantly as chaperones with low peroxidase activity. To better understand the regulation of cAPX, we characterized its structural conformation in the WT and NtCDC48-TAP lines through native-gel experiments (Fig. 7F). As control, a denaturing gel was performed and showed the predominance of the 33-kDa signal in overexpressing cells and of the 31-kDa signal in WT cells, as described above. In the native gels, cAPX was detected in HMW complexes in both the cell lines, as described in rice by Hong *et al.* (2018). In contrast, the dimer of cAPX (between 66–146 kDa) was only detected in WT cells. Thus, the overexpression of NtCDC48 negatively affects the presence of the cAPX dimer that harbours the main peroxidase activity.

### *Cellular redox status is affected in cells overexpressing NtCDC48*

As cAPX is a main regulator of the cellular redox status and, in contrast to WT cells, did not show induced activity in cryptogein-treated NtCDC48-TAP cells (Fig. 7C), a comparative analysis of the redox status was performed. We focused on glutathione, and measured the contents of total glutathione (GSH+GSSG) and of GSH after cryptogein treatment (Fig. 8A, B). In WT cells, the contents of both total and GSH slightly decreased after 12 h of elicitation with cryptogein. At each measurement time-point, we calculated the percentage of GSH and the GSH/GSSG ratio. Despite the decrease in total glutathione after 12 h, the percentage of GSH in the WT remained constant and it represented ~90% of the total glutathione pool (Fig. 8C). The GSH/GSSG ratio in WT cells displayed a slight and transient decline at 2 h, but otherwise was constant during elicitation (Fig. 8D). In the NtCDC48-TAP cells, more pronounced and significant decreases in total glutathione and in GSH were observed after 12 h of elicitation (Fig. 8A, B). The percentage of GSH was unaltered at 2 h of elicitation but then declined significantly to 42% of its initial value at 12 h (Fig. 8C). This decrease was accompanied by a drastic fall in the GSH/GSSG ratio from 20 to 2 (Fig. 8D).

As noted above, GR catalyses the reduction of GSSG to GSH and is necessary for regeneration of ascorbate. In WT cells, there were no significant differences in GR activity during the 12 h of exposure to cryptogein (Fig. 8E). However, in cells overexpressing NtCDC48, the GR activity had decreased at 2 h but then returned to the initial level at 12 h of treatment.

To determine whether the decrease of GSH in overexpressing cells could be linked to down-regulation of the expression of GSH synthases (GSH1 and GSH2) we measured the levels of *GSH1* and *GSH2* mRNA during cryptogein treatment (Fig. 9A). We found that the transcript levels did not change during elicitation in either of the cell lines, and thus the earlier decrease in GSH in the overexpressing cells could not be explained by the amount of GSH synthase transcripts.

As GSH can also be a substrate of glutathione-*S*-transferases (GST), we examined the amount of transcripts and the enzymatic activities of the tau and phi classes of GST, which are the most important forms in plants (McGonigle *et al.*, 2000; Nutricati *et al.*, 2006). The transcript levels of both these GST classes were significantly up-regulated in response to cryptogein from 4 h of treatment onwards in both WT and NtCDC48-TAP cells (Fig. 9B). GST activity was similar in both the cell lines, and was not affected by cryptogein elicitation (Fig. 9C). Taken together, these results indicated that the premature and more pronounced loss of glutathione in NtCDC48-TAP cells was not due to GST activity.

### *Heat shock affects induction of cAPX activity, but not cell death, in cells overexpressing NtCDC48*

To determine whether the differential regulation of cAPX observed between the WT and the NtCDC48-TAP lines was specific to cryptogein treatment, we investigated its accumulation and activity in response to exposure to flagellin 22 (flg22) or to heat shock (HS). The flg22 epitope of flagellin from bacteria activates intracellular immune signalling but not cell death in various plant species including tobacco (Zipfel *et al.*, 2004; Trdá *et al.*, 2014). In contrast to cryptogein, flg22 did not trigger cell death in the WT and NtCDC48-TAP cells (Supplementary Fig. S5A). At the protein level, as also observed for cryptogein, the 33-kDa signal was predominant in the overexpressing line (Fig. 10A). However, flg22 did not affect the accumulation of cAPX irrespective the cell line. Similarly, cAPX activity was not affected in either cell lines (Fig. 10C).

Exposure of WT and NtCDC48-TAP cells to HS at 55 °C for 10 min induced significant cell death (Supplementary Fig. S5B). Interestingly, in contrast to cryptogein treatment, the rates of HS-triggered cell death were similar in both lines. At the protein level, the 33-kDa cAPX signal was again predominant in the NtCDC48-overexpressing line (Fig. 10B). While HS did not affect the accumulation of cAPX in WT cells, in NtCDC48-TAP cells the amount of cAPX decreased dramatically just after the stress was applied and then gradually increased during the time course. Both lines also displayed distinct results with regard to cAPX activity. In WT cells, an increase of activity was observed at 4 h after HS and was maintained through to 12 h (Fig. 10D). An increase of cAPX activity was also observed in the overexpressing line, but it occurred later and was 88% and 63% lower than in the WT at 6 h and 12 h, respectively.

Thus, as was observed for cryptogein treatment, the induction of cAPX activity by HS was strongly affected in cells overexpressing NtCDC48. In contrast, cryptogein alone triggered faster and higher levels of cell death in the NtCDC48-TAP line (Supplementary Fig. S5C).

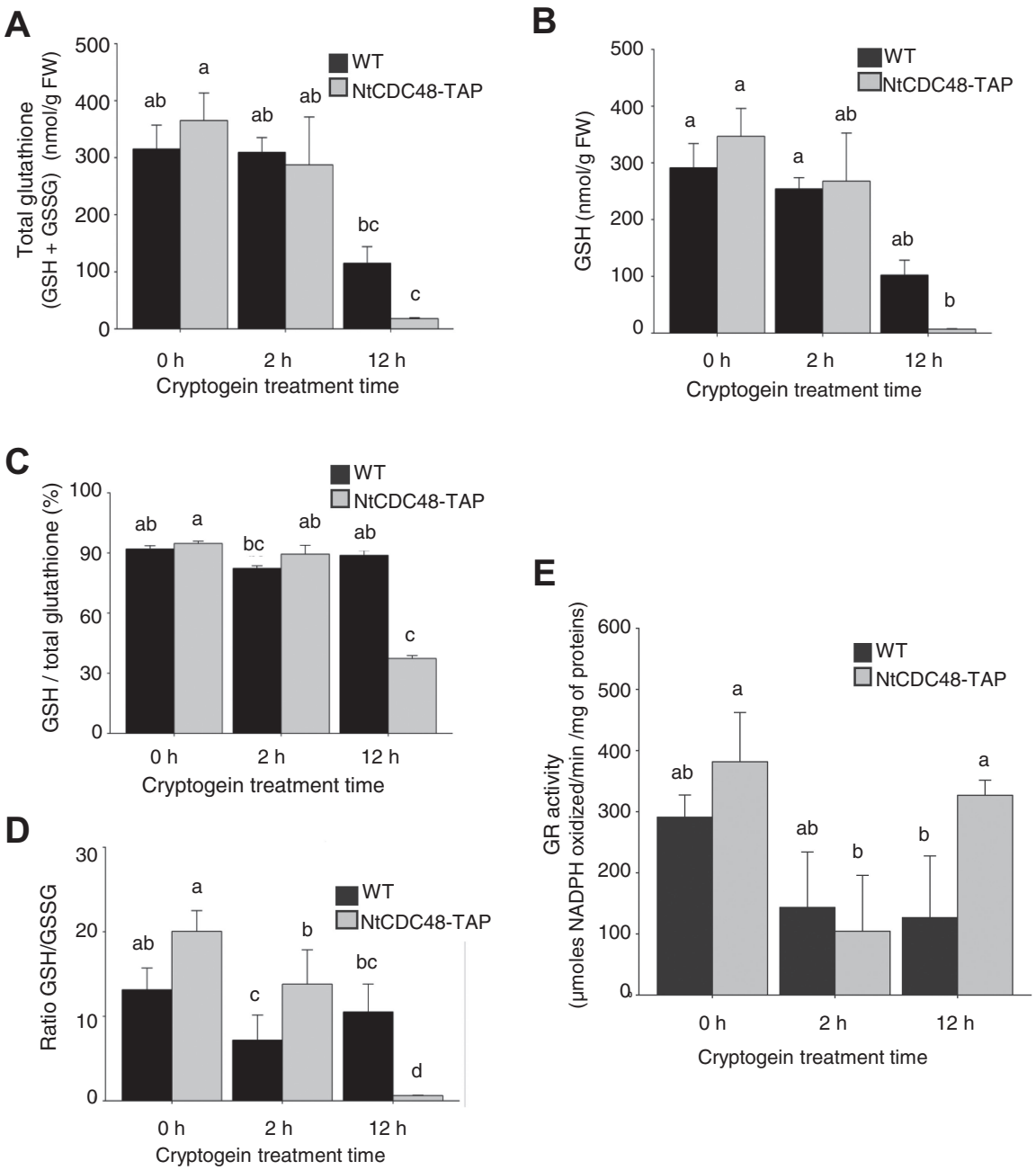


**Fig. 8.** Redox status in wild-type (WT) and NtCDC48-TAP tobacco cells. All experiments were performed on cells treated with 100 nM cryptogein for the period indicated. (A) Total glutathione content (GSH + GSSG), (B) reduced glutathione (GSH, deduced from GSSG and total glutathione), (C) percentage reduction of the glutathione pool: (GSH/total glutathione)×100, (D) the GSH/GSSG ratio, and (E) glutathione reductase (GR) activity. Data are means (±SE) of four biological replicates. Different letters indicate significant differences as determined using Kruskal–Wallis test ($P$<0.05).

## Discussion

The aim of this study was to investigate the involvement of NtCDC48 in the regulation of cAPX. We demonstrated that both proteins interact (Fig. 1), thus confirming our previous suggestion that cAPX could represent a target of NtCDC48 (Rosnoblet *et al.*, 2017). The interaction occurred independently of cryptogein treatment, suggesting that NtCDC48 contributes constitutively to cAPX turnover. In addition, although NtCDC48 was found both in the cytoplasm and in the nucleus, as previously reported (Park *et al.*, 2008), the interaction between the proteins occurred only in the cytosol (Fig. 2), in accordance with the expected subcellular localization of cAPX. Furthermore, cell fractionation experiments did not reveal any translocation of the proteins towards the nucleus during cryptogein elicitation (results not shown).

Accumulation of the cAPX transcript was enhanced in both WT and NtCDC48-TAP tobacco cells treated with cryptogein (Fig. 3A, B), indicating an induced expression of *cAPX* or a higher stabilization of the transcripts. The results also showed that the overexpression of NtCDC48 did not alter this process. A different situation occurred at the protein level. In WT cells, two immunoreactive bands with molecular masses of ~31 kDa and ~33 kDa were detected in immunoblots in

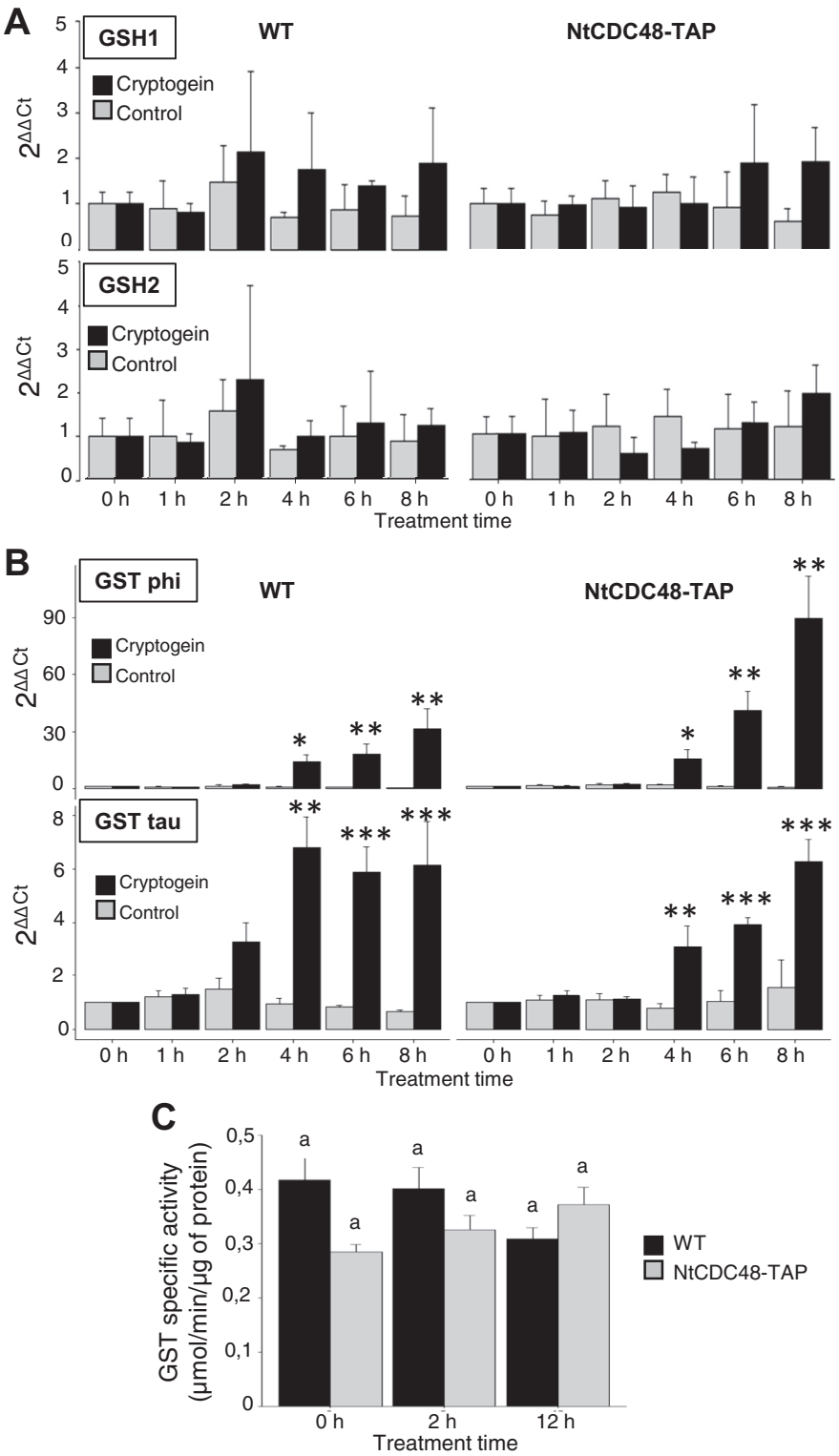


**Fig. 9.** Accumulation of *GSH synthases* and *GST* transcripts, and enzymatic activity of GST in wild-type (WT) and NtCDC48-TAP tobacco cells. (A, B) Amount of transcripts in cells elicited with 100 nM cryptogein. Accumulation of *GSH1* and *GSH2* (A) and *GST tau* and *phi* (B) was analysed by reverse-transcriptase quantification PCR (RT-qPCR) using *L25* mRNA as the calibrator gene. Data are means (±SE) of five independent experiments. Significant differences between treated and controls were determined using ANOVA test followed by Tukey's range test (**P*<0.05, ***P*<0.01, ****P*<0.001). (C) Enzymatic activity of GSTs (tau and phi) from WT and NtCDC48-TAP cells during cryptogein treatment. The substrate CDNB (1-chloro-2,4-dinitrobenzene) was used for the measurement of the GST activity by absorbance at 340 nm. Data are means (±SE) of four biological replicates. Statistical analysis was carried out using Kruskal–Wallis test: no significant differences were detected (*P*>0.05).

denaturing and reducing conditions (Fig. 3C). The accumulation of both signals was enhanced in response to cryptogein, with a higher stability of the 31-kDa band being observed over time. In contrast, in NtCDC48-overexpressing cells, the 33-kDa band was predominant while the 31-kDa band was either not or rarely detected. In addition, compared to WT

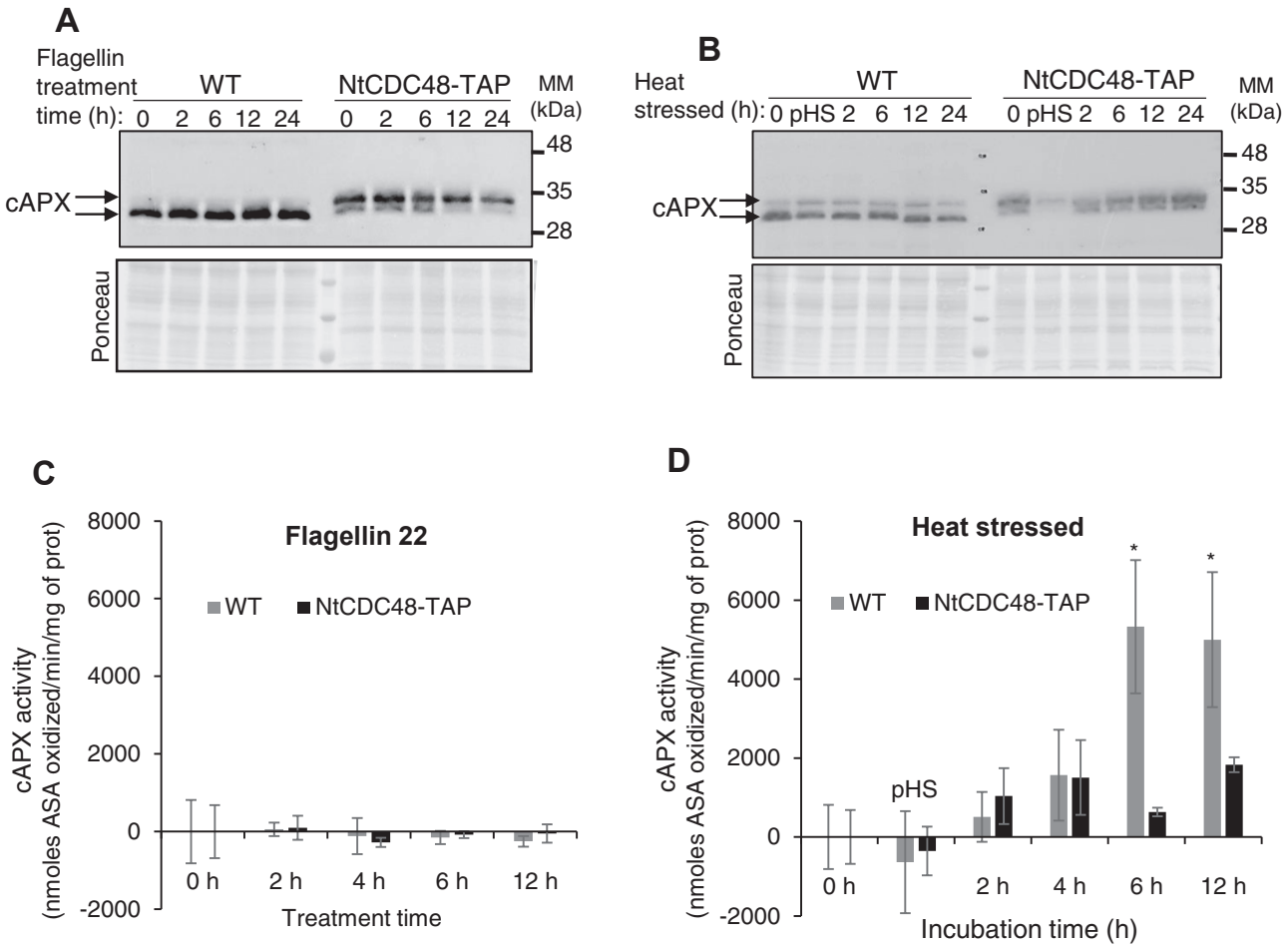


**Fig. 10.** cAPX protein amounts and activity during flagellin 22 (fgl22) elicitation and after heat shock (HS) in wild-type (WT) and NtCDC48-TAP tobacco cells. Cells were treated with 1 µM of flg22 or stressed by HS for 10 min at 55 °C (pHS, post heat shock). The treatment or incubation times after HS are indicated for each experiment. (A, B) Protein amounts of cAPX. Samples of 20 µg of proteins extracted from cells treated with flg22 (A) or from cells stressed by HS (B) were separated by SDS-PAGE and endogenous cAPX was analysed by immunoblotting (top panels). Protein loadings were checked using Ponceau staining (bottom panels). (C, D) cAPX enzymatic activity in WT and NtCDC48-TAP cells treated with flg22 (C) or after HS (D) after subtraction of control values. Significant differences between control and treated cells were determined using Wilcoxon's test (*$P$<0.05).

cells, we did not see an induction of the protein accumulation upon cryptogein treatment in the overexpressing line (Fig. 3C) . In addition, the cAPX dimer, which harbors the main cAPX activity (Hong *et al.*, 2018), was either absent or hardly detected in the overexpressing line (Fig. 7F). Thus, the overexpression of NtCDC48 significantly impacts the cAPX protein, both quantitatively and qualitatively.

How can these observations be interpreted? APX has been shown to be subject to PTM in the form of nitrosylation or phosphorylation (Correa-Aragunde *et al.*, 2015; Gou *et al.*, 2015), but the latter possibility was excluded by gel retardation assays (Fig. 4). In agreement with this, cAPX has been found amongst proteins undergoing constitutive *S*-nitrosylation in tobacco cells (Astier *et al.*, 2012). Whilst we confirmed the *in vitro S*-nitrosylation of cAPX and the consequent inhibition of its activity (Supplementary Fig. S3), as previously reported (de Pinto *et al.*, 2013), this PTM did not explain the appearance of the two immunoreactive signals. Moreover, the 33-kDa band was delayed in gel filtration (Fig. 6). Therefore, rather than there being an increase in mass, we assume that the presence of the 33-kDa band might reflect a PTM that slows down both electrophoretic mobility and elution by gel filtration. This could be due to oxidative modification. Supporting this hypothesis, the intensity of the 33-kDa band was reduced in favor of the 31-kDa signal when the protein extracts were exposed to NEM, a chemical agent that promotes alkylation of Cys residues (Paulech *et al.*, 2013; Fig. 5). Thus, the 33-kDa could correspond to a Cys-dependent PTM of cAPX that is up-regulated in the NtCDC48-overexpressing line. To confirm that the 33-kDa band was an oxidized isoform of cAPX, we tried to oxidize the recombinant protein *in vitro* using different approaches and we also examined the sulfenylation of the protein using IP and dedicated antibodies. However, none of these approaches were able to confirm the oxidation of cAPX.

The overexpression of NtCDC48 also altered cAPX activity, as the background and the induced activity triggered by cryptogein were reduced and impaired, respectively, as compared to WT cells (Fig. 7). The reduced activity observed in the transgenic line was not related to a lower ascorbate concentration. Nevertheless, we found that the dimeric structure of APX that harbors the main cAPX activity could not be detected in cells overexpressing NtCDC48. Therefore, it is reasonable

to assume that the reduced activity of cAPX could be related to the reduced abundance of the cAPX dimer. Given that the 33-kDa signal was predominant in NtCDC48-TAP cells, it might be hypothesized that this isoform of cAPX is not prone to dimerization, in contrast to the 31-kDa isoform that accumulated in WT cells.

Although we did not correlate the impairment of cAPX activity with the higher rate of cell death triggered by cryptogein in NtCDC48-TAP cells (Supplementary Fig. S5C), our results were in line with those of Mittler *et al.* (1999), who reported increased cell death in a transgenic tobacco line expressing antisense *APX* RNA infected by *Pseudomonas syringae* pv *phaseolicola*. Our results also raise the question of the ROS concentration. With regards to the role of cAPX in detoxification of $H_2O_2$, a higher level of this oxidant and, more generally, an alteration of the redox control, might be expected in the NtCDC48-TAP cells exposed to cryptogein. We have previously reported that the production of $H_2O_2$ induced in the apoplast is similar in the WT and NtCDC48-overexpressing lines (Rosnoblet *et al.*, 2017). As cryptogein also triggers an increase of ROS concentration in intracellular compartments (Allan and Fluhr, 1997), we tried to quantify its production in cell suspensions using the ROS-sensitive fluorescence probe fluorescein $H_2$DCF-DA or a luminol-based protocol; however, the results were poorly reproducible and could not be interpreted (results not shown). Nevertheless, we obtained interesting information from our measurements of the total glutathione content (GSH+GSSG) and the GSH/GSSG ratio (Fig. 8). First, in WT cells, the contents of both the reduced and oxidized forms of glutathione decreased at 12 h of cryptogein treatment. The percentage of GSH and the GSH/GSSG ratio remained constant from 0–12 h, with the ratio values being similar to those reported in Arabidopsis plantlets grown in air either with or without a high $CO_2$ concentration (Mhamdi *et al.*, 2010). According to Noctor *et al.* (2012), even though the GSH/GSSG ratio might remain unchanged, a decrease in glutathione concentration alone is sufficient to lead to a less-reducing environment for the plant cell. Thus, our data indicate that cryptogein triggered a modification in the redox status, and they also agree with a previous study that showed a significant reduction of the GSH concentration in tobacco leaves infiltrated with this elicitor (Davoine *et al.*, 2006). Second, whilst the basal state of glutathione in NtCDC48-overexpressing cells was equivalent to that of WT cells, after 12 h of cryptogein treatment, the decrease in content was more pronounced and the percentage of GSH and the GSH/GSSG ratio were also strongly decreased. Because GSH/GSSG ratios under 3:1 are indicative of a severe decrease in the cell capacity to respond to oxidative stress (Potters *et al.*, 2010), our results indicated that overexpression of NtCDC48 deeply affected the redox metabolism of cells facing the cryptogein-induced immune response. Furthermore, we showed that the decrease in GSH amount was neither linked to GST activities nor to GSH synthase gene expression, which could suggest an alteration in the activity of GSH synthase or its degradation in NtCDC48-TAP cells. We also cannot exclude the possibility that the absence of induction of cAPX activity in NtCDC48-TAP cells more or less directly explains the decrease in GSH level.

A key question arising from this study is whether the regulation of cAPX found in the transgenic line is specific to cryptogein. Several arguments do not support this possibility. First, the interaction between cAPX and NtCDC48 occurred in both untreated and elicited cells (Fig. 1). Second, the absence of the cAPX dimer in the overexpressing cells was observed in both untreated and in elicited cells (Fig. 7F). Third, compared to WT cells, the induction of cAPX activity in the overexpressing cells was strongly reduced in response to cryptogein but also after HS (Figs 7C, 10D). These observations therefore indicated that the reduced accumulation of the cAPX dimer as well as the impairment of cAPX inducible activity in the transgenic line were due to NtCDC48 overexpression and were unrelated to cryptogein or HS-induced effects. On the other hand, our data also indicated that the occurrence of overexpression of NtCDC48 on cell death differed according to the stimuli imposed. Thus, while the rate and pattern of HS-induced cell death were similar in WT and NtCDC48-TAP cells, cryptogein-induced cell death was exacerbated in the transgenic cells. This observation suggests that the involvement of NtCDC48 in the regulation of cell death is specific to cryptogein.

In conclusion, our results indicate a role for NtCDC48 in the regulation of cAPX at several levels and, more generally, provide evidence that the rate of NtCDC48 expression affects the overall glutathione status. As both catalase and ascorbate peroxidase have also been identified as putative partners of NtCDC48 (Rosnoblet *et al.*, 2017), it may represent a key regulator of the cellular redox status. Further studies are required to investigate this possibility.

## Supplementary data

Supplementary data are available at *JXB* online.

Table S1. List of primers used for PCR and RT-qPCR.

Fig. S1. The cAPX sequence from UniProtKB with matching peptides identified by MS analysis following co-IP of NtCDC48.

Fig. S2. The subcellular co-localization between cAPX and NtCDC48 in tobacco leaves double-agro-infiltrated with cAPX-YFP and CFP-NtCDC48.

Fig. S3. Analysis of recombinant cAPX *S*-nitrosylation.

Fig. S4. Comparison of total and cytosolic APX activities in WT cells treated with 100 nM cryptogein.

Fig. S5. Cell death in tobacco cells under elicitation with flagellin 22 and after heat shock.

## Acknowledgements

We thank DImaCell microscopy facilities, Graham Noctor for advice about redox state measurements, Agnès Klinguer for assistance with the cell culture, Maria Concetta de Pinto for providing the cAPX antibody, and Benoit Poinssot for providing flg22. Funding was provided by La Région Bourgogne (PARI AGREE) and the French Ministry of Higher Education, Research and Innovation (PhD scholarship to HB).

## References


**Allan AC, Fluhr R.** 1997. Two distinct sources of elicited reactive oxygen species in tobacco epidermal cells. The Plant Cell **9**, 1559–1572.

**Amako K, Chen G-X, Asada K.** 1994. Separate assays specific for ascorbate peroxidase and guaiacol peroxidase and for the chloroplastic and cytosolic isozymes of ascorbate peroxidase in plants. Plant & Cell Physiology **35**, 497–504.

**Anjum NA, Sharma P, Gill SS, *et al*.** 2016. Catalase and ascorbate peroxidase-representative $H_2O_2$-detoxifying heme enzymes in plants. Environmental Science and Pollution Research International **23**, 19002–19029.

**Asada K.** 1999. The water–water cycle in chloroplasts: scavenging of active oxygens and dissipation of excess photons. Annual Review of Plant Physiology and Plant Molecular Biology **50**, 601–639.

**Astier J, Besson-Bard A, Lamotte O, Bertoldo J, Bourque S, Terenzi H, Wendehenne D.** 2012. Nitric oxide inhibits the ATPase activity of the chaperone-like AAA+ ATPase CDC48, a target for S-nitrosylation in cryptogein signalling in tobacco cells. The Biochemical Journal **447**, 249–260.

**Baek GH, Cheng H, Choe V, Bao X, Shao J, Luo S, Rao H.** 2013. Cdc48: a Swiss Army Knife of cell biology. Journal of Amino Acids **2013**, 183421.

**Bai X, Yang L, Tian M, Chen J, Shi J, Yang Y, Hu X.** 2011. Nitric oxide enhances desiccation tolerance of recalcitrant *Antiaris toxicaria* seeds via protein S-nitrosylation and carbonylation. PLoS ONE **6**, e20714.

**Begara-Morales JC, Sánchez-Calvo B, Chaki M, Valderrama R, Mata-Pérez C, López-Jaramillo J, Padilla MN, Carreras A, Corpas FJ, Barroso JB.** 2014. Dual regulation of cytosolic ascorbate peroxidase (APX) by tyrosine nitration and S-nitrosylation. Journal of Experimental Botany **65**, 527–538.

**Bègue H, Jeandroz S, Blanchard C, Wendehenne D, Rosnoblet C.** 2017. Structure and functions of the chaperone-like p97/CDC48 in plants. Biochimica et Biophysica Acta General Subjects **1861**, 3053–3060.

**Besson-Bard A, Pugin A, Wendehenne D.** 2008. New insights into nitric oxide signaling in plants. Annual Review of Plant Biology **59**, 21–39.

**Bonnet P, Bourdon E, Ponchet M, Blein J-P, Ricci P.** 1996. Acquired resistance triggered by elicitins in tobacco and other plants. European Journal of Plant Pathology **102**, 181–192.

**Bradford MM.** 1976. A rapid and sensitive method for the quantitation of microgram quantities of protein utilizing the principle of protein–dye binding. Analytical Biochemistry **72**, 248–254.

**Chen LJ, Zou WS, Wu G, Lin HH, Xi DH.** 2018. Tobacco alpha-expansin EXPA4 plays a role in *Nicotiana benthamiana* defence against Tobacco mosaic virus. Planta **247**, 355–368.

**Clark D, Durner J, Navarre DA, Klessig DF.** 2000. Nitric oxide inhibition of tobacco catalase and ascorbate peroxidase. Molecular Plant-Microbe Interactions **13**, 1380–1384.

**Copeland C, Woloshen V, Huang Y, Li X.** 2016. AtCDC48A is involved in the turnover of an NLR immune receptor. The Plant Journal **88**, 294–305.

**Correa-Aragunde N, Foresi N, Lamattina L.** 2015. Nitric oxide is a ubiquitous signal for maintaining redox balance in plant cells: regulation of ascorbate peroxidase as a case study. Journal of Experimental Botany **66**, 2913–2921.

**Davoine C, Falletti O, Douki T, Iacazio G, Ennar N, Montillet JL, Triantaphylidès C.** 2006. Adducts of oxylipin electrophiles to glutathione reflect a 13 specificity of the downstream lipoxygenase pathway in the tobacco hypersensitive response. Plant Physiology **140**, 1484–1493.

**de Pinto MC, Locato V, Sgobba A, Romero-Puertas Mdel C, Gadaleta C, Delledonne M, De Gara L.** 2013. *S*-nitrosylation of ascorbate peroxidase is part of programmed cell death signaling in tobacco Bright Yellow-2 cells. Plant Physiology **163**, 1766–1775.

**Deruyffelaere C, Purkrtova Z, Bouchez I, Collet B, Cacas JL, Chardot T, Gallois JL, D'Andrea S.** 2018. PUX10 is a CDC48A adaptor protein that regulates the extraction of ubiquitinated oleosins from seed lipid droplets in Arabidopsis. The Plant Cell **30**, 2116–2136.

**Fujiwara A, Togawa S, Hikawa T, Matsuura H, Masuta C, Inukai T.** 2016. Ascorbic acid accumulates as a defense response to Turnip mosaic virus in resistant *Brassica rapa* cultivars. Journal of Experimental Botany **67**, 4391–4402.

**Gou JY, Li K, Wu K, *et al*.** 2015. Wheat stripe rust resistance protein WKS1 reduces the ability of the thylakoid-associated ascorbate peroxidase to detoxify reactive oxygen species. The Plant Cell **27**, 1755–1770.

**Hong SH, Tripathi BN, Chung MS, *et al*.** 2018. Functional switching of ascorbate peroxidase 2 of rice (OsAPX2) between peroxidase and molecular chaperone. Scientific Reports **8**, 9171.

**Karimi M, De Meyer B, Hilson P.** 2005. Modular cloning in plant cells. Trends in Plant Science **10**, 103–105.

**Kretzschmar FK, Mengel LA, Müller AO, Schmitt K, Blersch KF, Valerius O, Braus GH, Ischebeck T.** 2018. PUX10 is a lipid droplet-localized scaffold protein that interacts with CELL DIVISION CYCLE48 and is involved in the degradation of lipid droplet proteins. The Plant Cell **30**, 2137–2160.

**Lozano-Juste J, Colom-Moreno R, León J.** 2011. *In vivo* protein tyrosine nitration in *Arabidopsis thaliana*. Journal of Experimental Botany **62**, 3501–3517.

**Madhusudhan R, Ishikawa T, Sawa Y, Shigeoka S, Shibata H.** 2003. Characterization of an ascorbate peroxidase in plastids of tobacco BY-2 cells. Physiologia Plantarum **117**, 550–557.

**Mano S, Yamaguchi K, Hayashi M, Nishimura M.** 1997. Stromal and thylakoid-bound ascorbate peroxidases are produced by alternative splicing in pumpkin. FEBS Letters **413**, 21–26.

**McGonigle B, Keeler SJ, Lau SM, Koeppe MK, O'Keefe DP.** 2000. A genomics approach to the comprehensive analysis of the glutathione *S*-transferase gene family in soybean and maize. Plant Physiology **124**, 1105–1120.

**Mhamdi A, Hager J, Chaouch S, *et al*.** 2010. Arabidopsis GLUTATHIONE REDUCTASE1 plays a crucial role in leaf responses to intracellular hydrogen peroxide and in ensuring appropriate gene expression through both salicylic acid and jasmonic acid signaling pathways. Plant Physiology **153**, 1144–1160.

**Mittler R, Feng X, Cohen M.** 1998. Post-transcriptional suppression of cytosolic ascorbate peroxidase expression during pathogen-induced programmed cell death in tobacco. The Plant Cell **10**, 461–473.

**Mittler R, Herr EH, Orvar BL, van Camp W, Willekens H, Inze D, Ellis BE.** 1999. Transgenic tobacco plants with reduced capability to detoxify reactive oxygen intermediates are hyperresponsive to pathogen infection. Proceedings of the National Academy of Sciences, USA **96**, 14165–14170.

**Mittler R, Vanderauwera S, Gollery M, Van Breusegem F.** 2004. Reactive oxygen gene network of plants. Trends in Plant Science **9**, 490–498.

**Murshed R, Lopez-Lauri F, Sallanon H.** 2008. Microplate quantification of enzymes of the plant ascorbate–glutathione cycle. Analytical Biochemistry **383**, 320–322.

**Niehl A, Amari K, Gereige D, Brandner K, Mély Y, Heinlein M.** 2012. Control of *Tobacco mosaic virus* movement protein fate by CELL-DIVISION-CYCLE protein48. Plant Physiology **160**, 2093–2108.

**Noctor G, Mhamdi A, Chaouch S, Han Y, Neukermans J, Marquez-Garcia B, Queval G, Foyer CH.** 2012. Glutathione in plants: an integrated overview. Plant, Cell & Environment **35**, 454–484.

**Noctor G, Mhamdi A, Foyer CH.** 2016. Oxidative stress and antioxidative systems: recipes for successful data collection and interpretation. Plant, Cell & Environment **39**, 1140–1160.

**Noctor G, Reichheld JP, Foyer CH.** 2018. ROS-related redox regulation and signaling in plants. Seminars in Cell & Developmental Biology **80**, 3–12.

**Nutricati E, Miceli A, Blando F, De Bellis L.** 2006. Characterization of two *Arabidopsis thaliana* glutathione *S*-transferases. Plant Cell Reports **25**, 997–1005.

**Orvar BL, Ellis BE.** 1995. Isolation of a cDNA encoding cytosolic ascorbate peroxidase in tobacco. Plant Physiology **108**, 839–840.

**Park S, Rancour DM, Bednarek SY.** 2008. *In planta* analysis of the cell cycle-dependent localization of AtCDC48A and its critical roles in cell division, expansion, and differentiation. Plant Physiology **148**, 246–258.

**Paulech J, Solis N, Cordwell SJ.** 2013. Characterization of reaction conditions providing rapid and specific cysteine alkylation for peptide-based mass spectrometry. Biochimica et Biophysica Acta **1834**, 372–379.

**Potters G, Horemans N, Jansen MA.** 2010. The cellular redox state in plant stress biology – a charging concept. Plant Physiology and Biochemistry **48**, 292–300.

**Queval G, Noctor G.** 2007. A plate reader method for the measurement of NAD, NADP, glutathione, and ascorbate in tissue extracts: application to redox profiling during Arabidopsis rosette development. Analytical Biochemistry **363**, 58–69.

**Rosnoblet C, Bègue H, Blanchard C, Pichereaux C, Besson-Bard A, Aimé S, Wendehenne D.** 2017. Functional characterization of the chaperon-like protein Cdc48 in cryptogein-induced immune response in tobacco. Plant, Cell & Environment **40**, 491–508.

**Schmidt GW, Delaney SK.** 2010. Stable internal reference genes for normalization of real-time RT-PCR in tobacco (*Nicotiana tabacum*) during development and abiotic stress. Molecular Genetics and Genomics **283**, 233–241.

**Trdá L, Fernandez O, Boutrot F, *et al*.** 2014. The grapevine flagellin receptor VvFLS2 differentially recognizes flagellin-derived epitopes from the endophytic growth-promoting bacterium *Burkholderia phytofirmans* and plant pathogenic bacteria. New Phytologist **201**, 1371–1384.

**Vacca RA, de Pinto MC, Valenti D, Passarella S, Marra E, De Gara L.** 2004. Production of reactive oxygen species, alteration of cytosolic ascorbate peroxidase, and impairment of mitochondrial metabolism are early events in heat shock-induced programmed cell death in tobacco Bright-Yellow 2 cells. Plant Physiology **134**, 1100–1112.

**Wang Q, Song C, Li CC.** 2004. Molecular perspectives on p97-VCP: progress in understanding its structure and diverse biological functions. Journal of Structural Biology **146**, 44–57.

**Wendehenne D, Gao QM, Kachroo A, Kachroo P.** 2014. Free radical-mediated systemic immunity in plants. Current Opinion in Plant Biology **20**, 127–134.

**Xing S, Wallmeroth N, Berendzen KW, Grefen C.** 2016. Techniques for the analysis of protein–protein interactions *in vivo*. Plant Physiology **171**, 727–758.

**Zipfel C, Robatzek S, Navarro L, Oakeley EJ, Jones JD, Felix G, Boller T.** 2004. Bacterial disease resistance in Arabidopsis through flagellin perception. Nature **428**, 764–767.